Available online at website: https://journal.bcrec.id/index.php/bcrec

Bulletin of Chemical Reaction Engineering & Catalysis, 20 (4) 2025, 709-722

Original Research Article

Effect of Surface Stabilizers on the Optical Properties of ZnSe/ZnS:Mn/ZnS Nanocrystals

Thi Diem Bui[1]*, Quang Liem Nguyen[2], Nguyen Van Cuong[1], Trong Tang Nguyen[1]

[1]Faculty of Chemical Engineering, Industrial University of Ho Chi Minh City, Ho Chi Minh City 70000, Vietnam
[2]Institute of Materials Science, Vietnam Academy of Science and Technology, 18 Hoang Quoc Viet, Hanoi 10000, Vietnam.

Received: 26th July 2025; Revised: 8th October 2025; Accepted: 9th October 2025
Available online: 12th October 2025; Published regularly: December 2025

Abstract

In this study, we produced nano-sized, spherical ZnSe/ZnS:Mn/ZnS in a non-toxic aqueous solvent with surface stabilizers such as 3-mercaptopropionic acid (MPA), polyethylene glycol (PEG), and starch. These surface stabilizers aid to prevent agglomeration and passivation, thereby stabilizing the nanoparticle surface. ZnSe/ZnS:Mn/ZnS nanocrystals (NCs) are cubic in structure. Changing the surface stabilizer and doping Mn metal does not alter the structure of the ZnSe base material, but it boosts fluorescence efficiency by 2.2 - 3.9 times. The fluorescence efficiency of ZnSe/ZnS:Mn/ZnS MPA NCs using MPA stabilizer is 73.95%, which is higher than the fluorescence efficiency of ZnSe/ZnS:Mn/ZnS Starch NCs (57.35%) using Starch stabilizer and higher than the fluorescence efficiency of ZnSe/ZnS:Mn/ZnS PEG NCs (41.72%) using PEG stabilizer. ZnSe/ZnS:Mn/ZnS MPA NCs are originally assessed for their potential use in biomedical applications.

Keywords: Acid 3-mercaptopropionic; ZnSe/ZnS:Mn/ZnS; Surface stabilizers; Polyethylene glycol (PEG); Starch

How to Cite: Bui, T. D., Nguyen, Q. L., Cuong, N. V., Nguyen, T. T. (2025). Effect of Surface Stabilizers on the Optical Properties of ZnSe/ZnS:Mn/ZnS Nanocrystals. *Bulletin of Chemical Reaction Engineering & Catalysis*, 20 (4), 709-722. (doi: 10.9767/bcrec.20454)

Permalink/DOI: https://doi.org/10.9767/bcrec.20454

1. Introduction

Scientists have focused their research on semiconductor nanocrystals (NCs) in recent decades because to their distinct features when compared to bulk semiconductors [1,2]. Specifically, group II–VI semiconductor NCs are high quantum efficiency semiconductors with a straight band gap [1,3]. ZnSe NCs are one of the least hazardous (Cd-free) and chemically stable II-VI semiconductors [4]. ZnSe possesses exceptional optical and electrical properties [5–7], making it suitable for a wide range of applications such as light-emitting devices, solar cells, chemical sensors, biomedicine, photocatalysis, and energy storage [8–10]. However, because to the difference in configuration between Zn and Se, there are certain flaws in ZnSe (Zn belongs to group IIB, Se belongs to group VIA), resulting in a low fluorescence efficiency. Furthermore, the suspension bonds on the surface of NCs produce trap states, influencing the fluorescence and quantum efficiency of NCs [11,12].

Additionally, II-VI semiconductor NCs are unstable aggregates or can aggregate exceedingly quickly due to the lack of a trapping medium, some sort of packing, or the particles' uncontrolled development [13,14]. Surface passivation has a substantial influence on nanocrystals' optoelectronic capabilities. These surface states are improved by connecting stabilizers to nanocrystals [15,16]. In general, electrostatic stabilization and steric hindrances can inhibit nanoparticle aggregation.

* Corresponding Author.
Email: buithidiem@iuh.edu.vn (T.D. Bui)

As a result, stabilizers are utilized in the synthesis of NCs to keep their form and nano size while also assisting NCs in increasing their volume and surface area [17,18]. To retain the structural features of the generated NCs, numerous capping agents, such as thiophenol, thiourea [19], glutathione (GSH) [20], and thioglycolic acid (TGA) [21], have been explored for semiconductor fabrication [22,23]. However, they are toxic, harmful to the environment, and have structures that are unsuitable for nanocrystals synthesis. For example, a 3-mercaptopropionic Acid (MPA) molecule can bind with a metal atom site to produce the optimal hexagonal configuration, increasing the colloidal stability of the resultant NCs. TGA is one methylene unit shorter than MPA; nonetheless, in order to produce the desired hexagonal structure, a TGA molecule must cover two metal atom sites with its carboxylate group. This coordination ability causes TGA to adsorb free metal ions in the surrounding medium and thus accelerates the crystal growth, which is not beneficial to the optical properties of the NCs.

The arguments listed above suggest that we should investigate green techniques for manufacturing NCs utilizing non-toxic, structurally distinct surfactants. The first ingredient is starch [24]. Starch is a branching substance made up of two major components: Amylose and Amylopectin. Amylose and Amylopectin ratios have a significant impact on starch characteristics [25,26]. Amylose is a linear polysaccharide made of glucose units connected by α-1,4-glycosidic linkages. Several research have also shown that this polysaccharide has biomedical applications, such as a substrate for cell spreading, a structure for tissue engineering, a mechanism for medication administration, and implants. Amylopectin shares the same backbone structure as amylose but contains more α-1,6 branch points. This polymer is extremely biocompatible and rapidly biodegradable [27]. Starch is widely used in many biomedical applications, ranging from topical skin release [28] to degradable drug microsphere carriers [29].

The second is PEG, a long linear polyether chain that can absorb water and form hydrogen bonds, allowing it to dissolve in polar solvents and stable the colloid in acidic or basic pH settings [30]. PEG is a low-toxicity polymer [31], biocompatible, and can be used for medical applications. Excellent water solubility [88], exceptionally low immunogenicity and antigenicity [32]. PEG is a non-biodegradable polymer that is rapidly excreted by biological beings. Its presence in aqueous solution has no negative impact on protein structure or enzyme activity [33]. When injected into animals, PEG maintains excellent stability in the blood compartment while accumulating minimally in the liver and spleen. Furthermore, PEG possesses conformational flexibility and good water binding properties [34,35]. As a result, this polymer has gained widespread acceptance for biomedical applications.

Finally, mercaptopropionic acid (MPA) has a short linear chain structure, making it an ideal surface stabilizer since its structure allows it to establish bonds with nanoparticle surface atoms and complexes with doped metal ions. Furthermore, the hydrophilic carboxylic groups on the outer surface of the NCs provide good water solubility once the thiol groups connect with the zinc and manganese ions on their surfaces [36]. Because of this capacity, MPA is frequently used as a capping ligand in the synthesis of ZnSe or other II-VI semiconductor NCs in aqueous solvents [37,38].

In this study, we investigated the green synthesis of ZnSe/ZnS:Mn/ZnS NCs based on non-toxic Zn, using water as solvent, low temperature synthesis (80-100 °C), and using low-toxic surface stabilizers with different structures such as MPA (short linear chain substance), PEG (long linear chain substance), and Starch (straight and branched chain substance) to investigate the influence of surface stabilizers on the properties and applicability of NCs in the bio.

2. Materials and Methods

2.1 Materials

High-purity chemical reagents are used for the synthesis of ZnSe/ZnS:Mn/ZnS NCs and their doped counterparts. Zinc acetate dihydrate ($Zn(CH_3COO)_2 \cdot 2H_2O$, Merck) was used as the Zn precursor, Mangan acetat ($Mn(CH_3COO)_2.4H_2O$, Merck) served as the Mn source, Sodium sulfide nonahydrate ($Na_2S.9H_2O$, Merck) served as the S source, Selenium powder (Se, Merck) and Natri borohydride ($NaBH_4$, Merck) served as the Se source. 3-Mercaptopropionic acid (MPA, Merck), polyethylene glycol (PEG, Merck), Starch (Merck) was employed as a stabilizing agent to enhance the solubility and stability of NCs in aqueous media. Ammonium hydroxide (NH_4OH, Merck) was used to adjust the pH of the reaction mixture to ensure the optimal conditions for NCs formation. Deionized (DI) water was used throughout the synthesis process to maintain the purity of the samples.

2.2. Synthesis of ZnSe/ZnS:Mn/ZnS NCs with MPA (or PEG, Starch) Surface Stabilizer

Stage 1: The core of ZnSe synthesis: In a 250 mL flask, mix 50 mL of 0.1 N MPA (or PEG, Starch) surface stabilizer, 90 mL of water, and 10 mL of 0.1 M Zn^{2+}. For fifteen minutes, whisk the mixture. Next, 2 M NH_4OH was used to raise the pH to 7. After adding the combined solution to the

NaHSe (In a vacuum, Se powder, $NaBH_4$, and water are combined to form NaHSe. Weigh 0.084 g of Se and 0.086 g of $NaBH_4$ in the reaction vessel, then remove all of the air. Quickly inject 3.0 ml of distilled water into the reaction vessel, the reaction occurs promptly to form a clear solution, and we obtain NaHSe solution), the solution maintained a temperature of 90 °C for three hours. Throughout the synthesis process, N_2 gas is supplied into the reaction system on a continuous basis to remove O_2 from the vessel.

Stage 2: Coating process of ZnS:Mn buffer shell and ZnS shell for ZnSe core: After the ZnSe core was synthesized, 7 mL of 0.1 M Zn^{2+} solution and 5 mL of 0.01 M Mn^{2+} solution were added at a drip rate of 1 drop per second to create the buffer shell (ZnS:Mn), which is coated on the outside of the core layer (ZnSe). Then, 7 mL of 0.1 M S^{2-} solution was gradually added to the reaction system. For one and a half hours, the system was heated to 80 °C while being stirred. We added 7 milliliters of 0.1 M Zn^{2+} solution and 7 milliliters of 0.1 M S^{2-}solution while stirring the reaction system for the next sixty minutes. Following the reaction, the system was cooled to complete it. The product was incubated for 24 hours before being rinsed with acetone 2-3 times, dried naturally, and prepared for analysis

2.3. Characterization of Materials

The structure of NCs was studied using X-ray diffraction (XRD) patterns (D8 ADVANCE, Germany) and high-resolution transmission electron microscopy (HRTEM) (JEM-2100, Japan). Optical NC characteristics including as UV-Vis absorption spectrum, PL, and Fourier-transform infrared spectroscopy (FTIR) were measured using a Cary 3500 Multicell UV-Vis Spectrophotometer, Cary Eclipse Fluorescence Spectrometer, and Bruker Tensor 27. EDS and STEM were used to identify the element. The chemical bonding of NCs was recorded using an X-ray photoelectron spectroscopy (XPS) spectrum (ESCALab250XI, Thermo Fisher Scientific). All measurements were done at room temperature.

2.4. Applications of Nanocrystals in Biomedicine

By affixing protein A and antibodies to luminous nanocrystals, the substance was examined for toxicity against the bacteria *E.coli O157:H7*. The bacteria were cultivated on liquid-specific media for an entire night before being diluted in physiological saline to progressively lower concentrations. The bacterial strains were placed at various concentrations in 6mm-diameter holes on the agar plate. Fill the well with 20 mm of NCs solution and incubate it at 37 °C for 24 hours. To ensure sensitivity, samples of NCs that are harmful to *E. coli O157:H7* bacteria were chosen for additional testing. The bacterial solution (100 µl) was treated with 20 µl of complexes incorporating EDC (1-ethyl-3-(3-dimethylaminopropyl)-carbodiimide hydrochloride), Protein A, and NCs beads and incubated at 4 °C for 5 hours. *E. coli O157:H7* was diluted. The entire system was incubated at 4 °C overnight. The capacity of protein A and bacteria to attach to the material beads was then assessed using light [39,40].

3. Results and Discussion

3.1. Structured Research

XRD analysis of ZnSe/ZnS:Mn/ZnS MPA NCs, ZnSe/ZnS:Mn/ZnS PEG NCs, and ZnSe/ZnS:Mn/ZnS Starch NCs synthesized employing different surface stabilizers all have cubic crystal structure (zinc blende) because they show diffraction peaks at 27.47°, 45.11°, and 53.97° corresponding to planes (111), (220), and (311), respectively, in line with standard card JCPDS 012-6803. Using alternative surface stabilizers and Mn doping under the examined conditions with a 5% Mn^{2+}/Zn^{2+} concentration had no effect on the crystalline phase composition. These results are highly consistent with those of other published investigations [41–43]. Interestingly, when Mn was added to ZnSe, the diffraction peaks migrated somewhat towards a lower 2-theta angle (Figure 1). Mn^{2+} has a greater ionic radius (0.8 Å) than Zn^{2+} (0.74 Å), suggesting that Mn^{2+} ions were used instead of Zn^{2+} ions during sample synthesis [44,45]. XRD results indicated no diffraction peaks for Mn metals or other compounds. As a result, it may be believed that Mn was successfully doped into ZnSe without causing structural changes. In which Mn^{2+} ions replaced Zn^{2+} ions or passed through lattice defects.

In addition, the XRD results of ZnSe/ZnS:Mn/ZnS MPA NCs showed sharper and higher diffraction peaks than those of ZnSe/ZnS:Mn/ZnS Starch NCs and ZnSe/ZnS:Mn/ZnS PEG NCs. The Full Width at Half Maximum peak width of ZnSe/ZnS:Mn/ZnS MPA NCs was narrower than that of ZnSe/ZnS:Mn/ZnS Starch NCs and ZnSe/ZnS:Mn/ZnS PEG NCs. This demonstrates that ZnSe/ZnS:Mn/ZnS MPA NCs have a stable, flawless crystal structure with few flaws, which is more uniform, compact, and uniform than ZnSe/ZnS:Mn/ZnS Starch NCs and ZnSe/ZnS:Mn/ZnS PEG NCs. The selected area electron diffraction (SEAD) pattern indicates that ZnSe is a polycrystallin with high crystallinity (Figure 1).

3.2. Compositional Studies

This To determine the presence and ratio of elements in the samples, we examined their EDX spectrum (Figure 2). The presence of Zn, Se, S and

the doped metal Mn in the samples is plainly visible, with recognizable peaks at the appropriate energies. MPA. PEG, Starch contains the elements C and O, which have been bound to the surface of the NCs. However, the actual value of the Mn^{2+}/Zn^{2+} element ratio is always less than the theoretical value, indicating that there are still a significant number of metal ions that cannot replace Zn^{2+} ions and are removed during sample cleaning. Furthermore, several extraneous elements do not appear in the spectrum image, demonstrating the great purity of the produced ZnSe/ZnS:Mn/ZnS NCs.

To identify the functional groups in the NCs, FT-IR spectra were collected. FT-IR spectrum of MPA and ZnSe/ZnS:Mn/ZnS MPA NCs samples Figure 3a shows PEG and ZnSe/ZnS:Mn/ZnS PEG NCs Figure 3b shows Starch and ZnSe/ZnS:Mn/ZnS Starch NCs Figure 3c, synthesized with a reaction time of 3 hours, demonstrates that the vibrational peaks corresponding to wavenumbers 3430 cm^{-1} and 3120 cm^{-1} are characteristic vibrations of O-H bonds and water adsorbed on the material surface. [46]. The peak at 2880 cm^{-1} corresponds to the vibration of the $-CH_2$ group bond. The peaks at 1623 cm^{-1} and 1710 cm^{-1} correspond to the vibration of the carboxyl group bond (-C=O) of PEG and MPA. The peaks at 1370 cm^{-1} and 990 cm^{-1} correspond to the vibrations of Starch's carboxyl group (-C-O) and C-C bonds in neutral medium, and they shift to 1730 cm^{-1} in alkaline media. The peaks at 2650 cm^{-1} and 2690 cm^{-1}

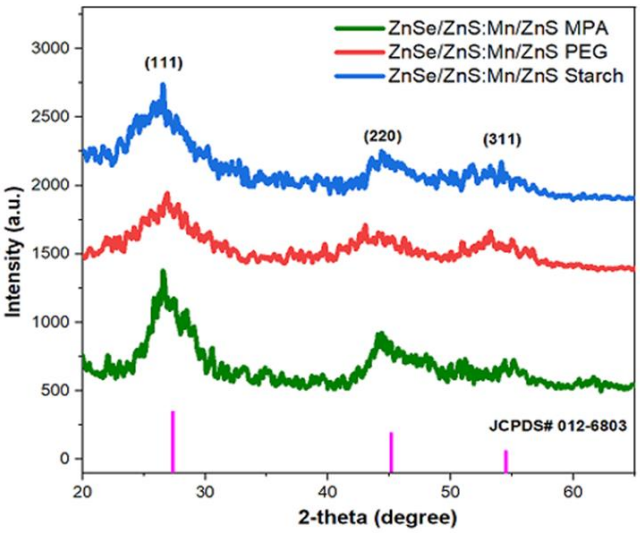

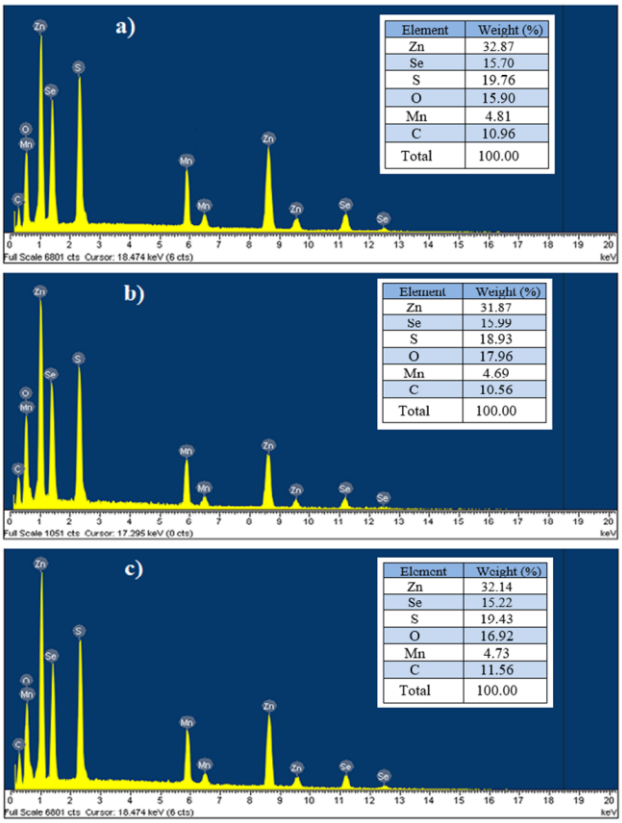

Figure 2. EDX spectra of ZnSe/ZnS:Mn/ZnS MPA NCs a), ZnSe/ZnS:Mn/ZnS PEG NCs b), ZnSe/ZnS:Mn/ZnS Starch NCs c) synthesized using different surface stabilizers.

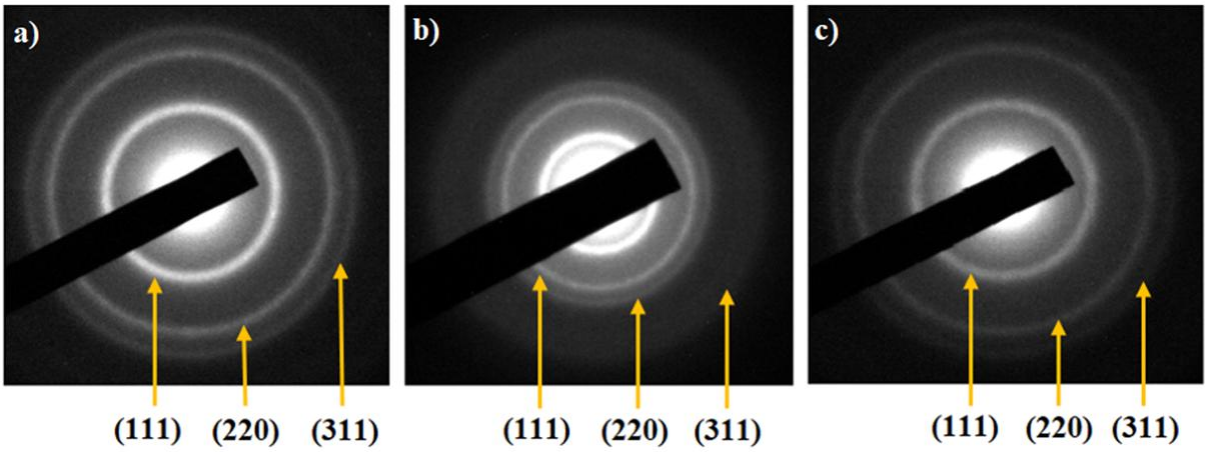

Figure 1. The XRD results of ZnSe/ZnS:Mn/ZnS MPA, ZnSe/ZnS:Mn/ZnS PEG, ZnSe/ZnS:Mn/ZnS Starch NCs with Mn^{2+}/Zn^{2+} ratio 5% and SEAD of ZnSe/ZnS:Mn/ZnS MPA: a), ZnSe/ZnS:Mn/ZnS PEG; b), ZnSe/ZnS:Mn/ZnS Starch; c) NCs synthesized using different surface stabilizers.

represent the distinctive vibrations of the S-H bond [47,48]. The peaks at 1110 cm^{-1} to 475 cm^{-1} represent the distinctive vibrations of the Zn-S bond [49,50].

To identify the functional groups in the NCs, FT-IR spectra were collected. FT-IR spectrum of MPA and ZnSe/ZnS:Mn/ZnS MPA NCs samples Figure 3a shows PEG and ZnSe/ZnS:Mn/ZnS PEG NCs Figure 3b shows Starch and ZnSe/ZnS:Mn/ZnS Starch NCs Figure 3c, synthesized with a reaction time of 3 hours, demonstrates that the vibrational peaks corresponding to wavenumbers 3430 cm^{-1} and 3120 cm^{-1} are characteristic vibrations of O-H bonds and water adsorbed on the material surface. [46]. The peak at 2880 cm^{-1} corresponds to the vibration of the -CH_2 group bond. The peaks at 1623 cm^{-1} and 1710 cm^{-1} correspond to the vibration of the carboxyl group bond (-C=O) of PEG and MPA. The peaks at 1370 cm^{-1} and 990 cm^{-1} correspond to the vibrations of Starch's carboxyl group (-C-O) and C-C bonds in neutral medium, and they shift to 1730 cm^{-1} in alkaline media. The peaks at 2650 cm^{-1} and 2690 cm^{-1} represent the distinctive vibrations of the S-H bond [47,48]. The peaks at 1110 cm^{-1} to 475 cm^{-1} represent the distinctive vibrations of the Zn-S bond [49,50].

As a result, the -S-H functional group of MPA is no longer present, but the -OH and -C=O vibration peaks of the -COOH group of MPA remain, indicating that MPA has linked to NCs and -SH has formed bonds on their surfaces. PEG's -OH, -CH, -C-O-C, and -C=O peaks remain unchanged. It is demonstrated that there is a bond formation between NCs and PEG, but the -OH, C-C, -CH_2, and -CO vibration peaks of starch are still present, showing that there is a bond formation on the surface between NCs and starch. These bonds increase the dispersibility of NCs in water, allowing them to be used in a variety of applications, including biology.

The single HrTEM images of ZnSe/ZnS:Mn/ZnS particles synthesized using MPA, PEG, and Starch surface stabilizers are observed in Figure 4a, d, and g, respectively, and the high-resolution TEM images of the shell are observed in Figure 4b-c, Figure 4e-f, and Figure 4h-i, respectively, which clearly show the (220) atomic plane of ZnS and the (111) atomic plane of ZnSe with lattice spacing of 0.23 nm and 0.32 nm for ZnSe/ZnS:Mn/Zn. Nanocrystals are spherical in form.

Figure 5 depicts the energy dispersive X-ray (EDX) spectra obtained using scanning transmission electron microscopy (STEM) of an

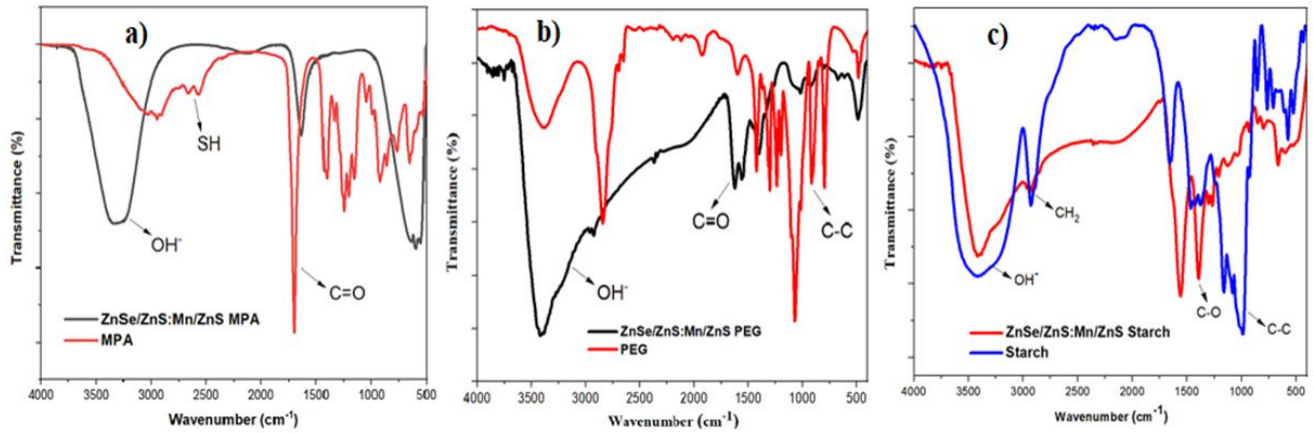

Figure 3. FT-IR spectrum of ZnSe/ZnS:Mn/ZnS MPA NCs a), ZnSe/ZnS:Mn/ZnS PEG b) and ZnSe/ZnS:Mn/ZnS Starch NCs produced with different surface stabilizers.

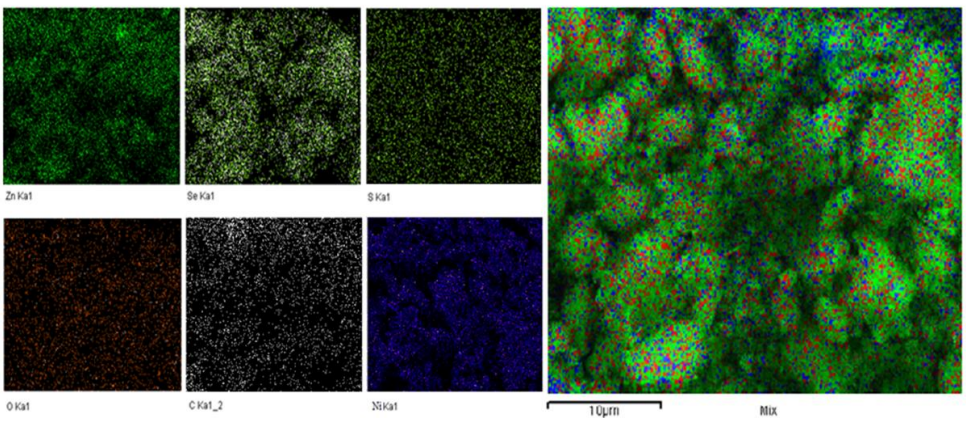

Figure 5. EDX-STEM of ZnSe/ZnS:Mn/ZnS NCs produced with MPA surface stabilizers.

example ZnSe/ZnS:Mn/ZnS MPA sample. Zinc (Zn), sulfur, and selenium (Se) atoms were found throughout the particle. Additionally, the presence of Mn, O, and C in ZnSe/ZnS:Mn/ZnS was established. The absence of extraneous components suggests that the nanocrystals were manufactured with great purity.

The XPS spectrum of ZnSe/ZnS:Mn/ZnS MPA NCs (Figure 6) reveals the presence of components in the representative sample, including Zn, Mn, O, C, S, and Se. The chemical states of these elements were resolved using an XPS spectrum in high resolution scan mode (Figure 6). This spectrum exhibits peaks at 1021.6 eV and 1044.8 eV, which indicate the binding energies of Zn $2p_{3/2}$ and Zn $2p_{1/2}$, respectively, representing the binding energy of Zn in the +2 oxidation state [51,52]. The peak at 527.3 eV is the binding energy of O 1s. The C 1s state found at binding energies 289.6 and 285.6 eV is associated with C-OH and O-(C=O) bonds. The peaks here are associated to C-O and O-(C=O) bonds in the lattice, therefore it can be anticipated that Zn is chemically bonded to C-O and C-OH [53]. The binding energies of 161.4 eV and 162.6 eV characterize the binding energies of S $2p_{3/2}$ and $2p_{1/2}$, which characterize the binding energy of S with state oxidizing 2, respectively, and the S-2p peak situated at 161.2 eV is attributable to the Zn-S bond [54], proving the successful formation of ZnS shell. The binding

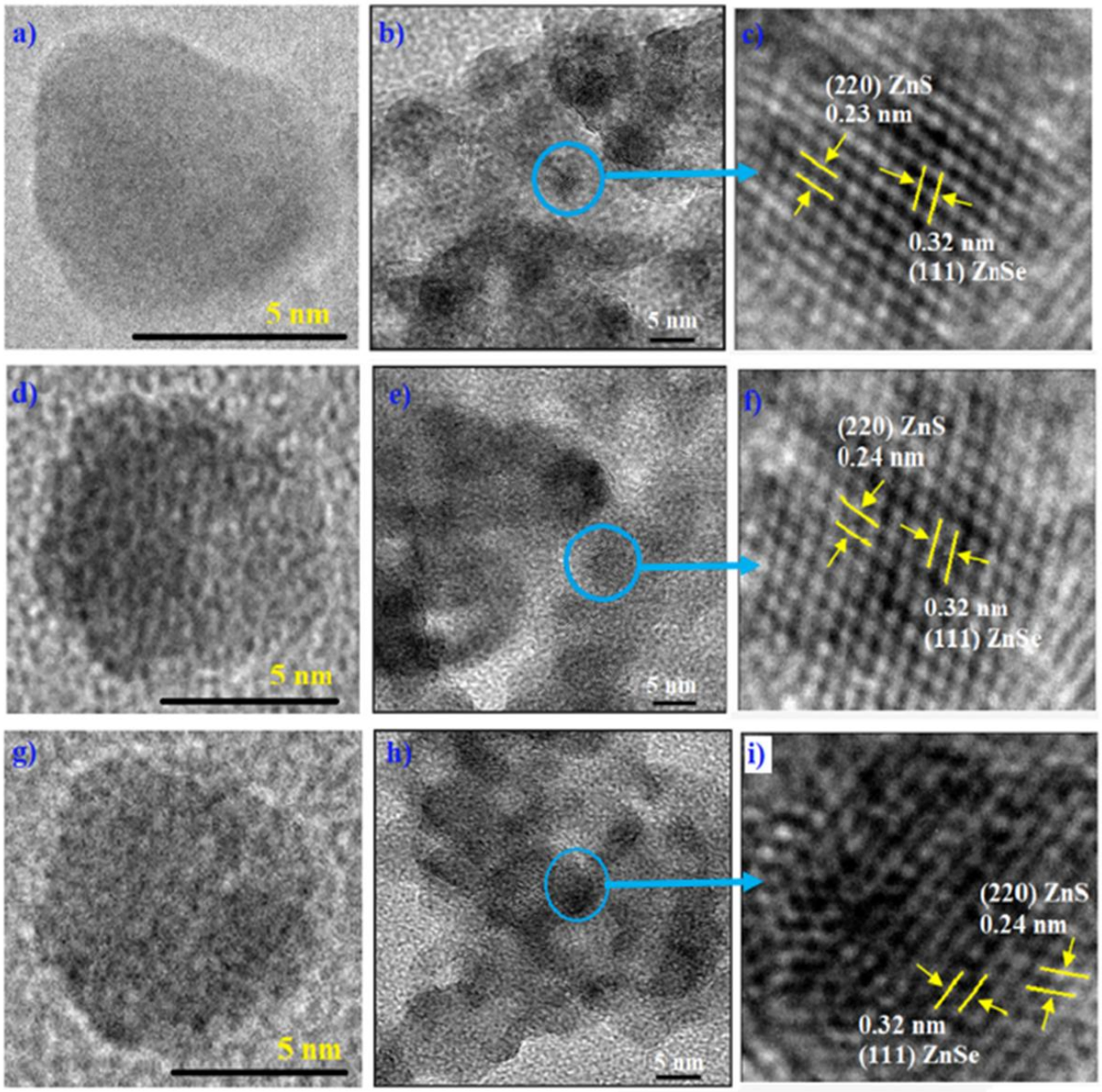

Figure 4. a) HrTEM of single of the ZnSe/ZnS:Mn/ZnS MPA particle, d) HrTEM of single of the ZnSe/ZnS:Mn/ZnS PEG particle, g) HrTEM of single of the ZnSe/ZnS:5%Mn/ZnS Starch particle, b,c) TEM of the ZnSe/ZnS:Mn/ZnS MPA NCs, e,f) TEM of the ZnSe/ZnS:Mn/ZnS PEG NCs, h,i) TEM of the ZnSe/ZnS:Mn/ZnS Starch NCs.

energy level of 640.6 eV characterizes the binding energy of Mn-$2p_{3/2}$ for the +2 oxidation state of Mn [55]. The intensity of the modest Mn-$2p_{3/2}$ spectral peak indicated that the sample contained little Mn^{2+}. Thus, Zn^{2+} ions existed in the ZnSe/ZnS:Mn/ZnS sample, indicating that manganese was successfully doped into the ZnS lattice. The Se 3d peaks in Figure 6(d) can be separated into two overlapping peaks, Se $3d_{5/2}$ and Se $3d_{3/2}$, at binding energies of 53.6 eV and 54.5 eV, respectively, reflecting Se 3d in Zn-Se. Thus, the representative sample contains Mn^{2+} ions, and Mn^{2+} has been successfully doped into the ZnSe crystal lattice. Mn^{2+} and Zn^{2+} ions have the same charge and similar radii, therefore Mn^{2+} ions can easily replace Zn^{2+} ion sites or occupy cation holes in the crystal lattice.

3.3. Optical Properties

UV-Vis absorption spectroscopy is a powerful method for studying the effect of doping on the optical properties of ZnSe/ZnS:Mn/ZnS NCs. Figure 7 depicts the absorption spectrum of ZnSe/ZnS:Mn/ZnS NCs. The UV-Vis spectra of ZnSe/ZnS:Mn/ZnS MPA NCs, ZnSe/ZnS:Mn/ZnS PEG NCs, and ZnSe/ZnS:Mn/ZnS starch NCs (Figure 7) revealed that the absorption edge of ZnSe/ZnS:Mn/ZnS starch NCs was slightly shifted to longer wavelengths when compared to ZnSe/ZnS:Mn/ZnS PEG NCs and ZnSe/ZnS:Mn/ZnS MPA NCs synthesized under the same conditions. This showed that ZnSe/ZnS:Mn/ZnS starch NCs were larger than ZnSe/ZnS:Mn/ZnS PEG NCs and ZnSe/ZnS:Mn/ZnS MPA NCs.

When exposed to UV light at 365 nm, the ZnSe/ZnS:Mn/ZnS NCs doped with Mn metal at a molar ratio of 5% Mn^{2+}/Zn^{2+} and utilizing different

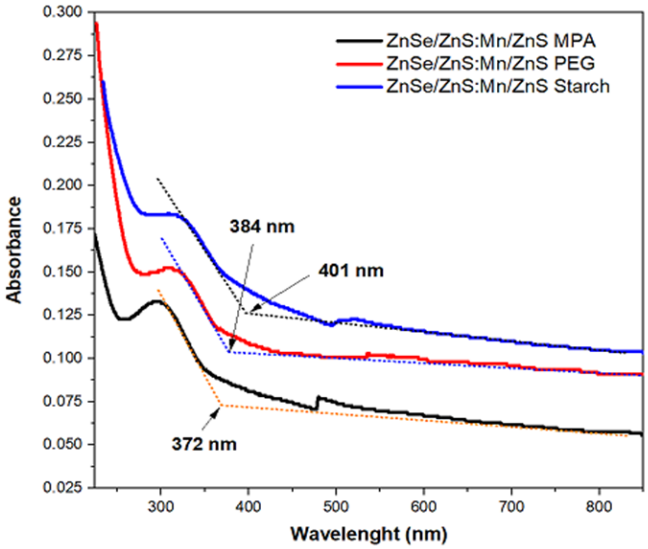

Figure 7. UV-Vis spectra of ZnSe/ZnS:Mn/ZnS MPA NCs, ZnSe/ZnS:Mn/ZnS PEG NCs, ZnSe/ZnS:Mn/ZnS Starch NCs synthesized using different surface stabilizers.

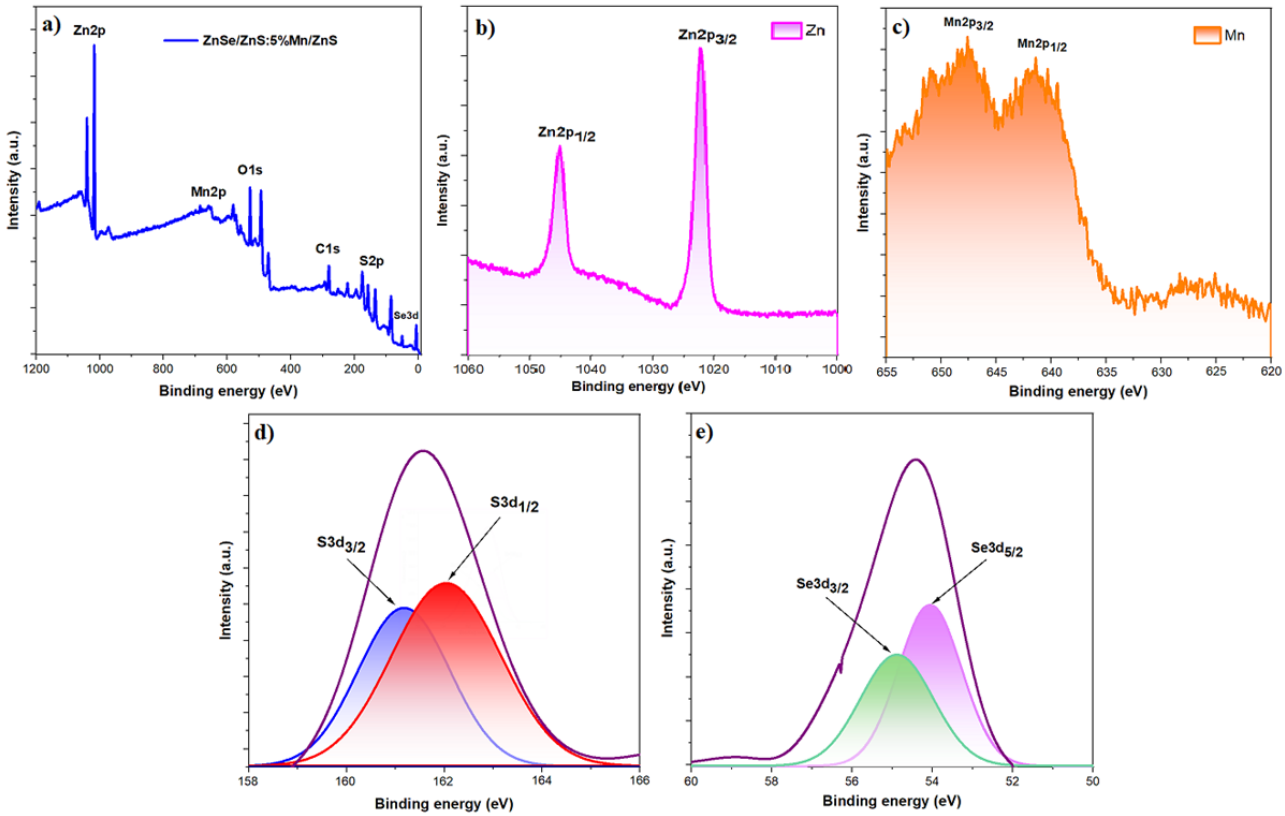

Figure 6. XPS spectrum of a) ZnSe/ZnS:Mn/ZnS MPA NCs, b) Zn 2p peak, c) Mn 2p peak, d) S 3d, and e) Se3d peak.

stabilizers produced the colors shown in Figures 8a, b, and c, respectively. When exposed to UV light at 365 nm, the ZnSe/ZnS:Mn/ZnS NCs emitted distinct orange-yellow light based on CIE chromaticity coordinates (Figure 8d). When tested under UV light, the MPA ZnSe/ZnS:Mn/ZnS NCs demonstrated the highest luminescence intensity in the series (Figure 8a).

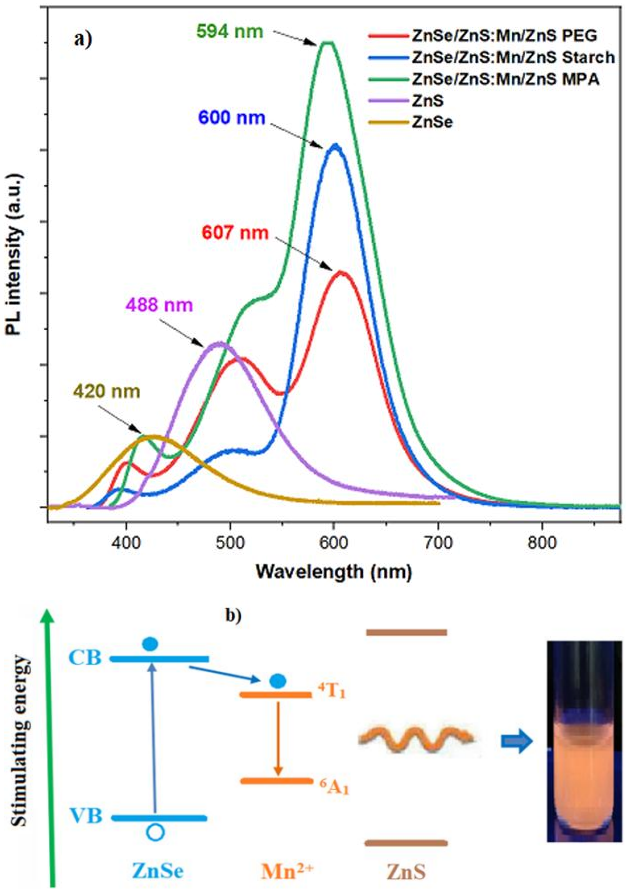

Figure 9. a) PL spectrum of ZnSe, ZnS, ZnSe/ZnS:Mn/ZnS MPA, ZnSe/ZnS:Mn/ZnS PEG, ZnSe/ZnS:Mn/ZnS Starch NCs and b) Schematic representation of the transition from the Mn^{2+} $^4T_1$ state to the $^6A_1$ state, which results in the orange-yellow light emission of ZnSe/ZnS:Mn/ZnS NCs.

In general, the maximum fluorescence efficiency is exactly proportional to the minimum density of surface-trap states on NCs [56,57]. Overgrowth with a shell that has a wider band gap than the core is an essential approach for improving the surface passivation of NCs [58] As a result, both electrons and holes are trapped in the core, which improves radiative recombination (Figure 9b). The PL spectrum of ZnSe/ZnS:Mn/ZnS NCs produced using different surface stabilizers (Figure 9) displays three peaks: the peak at 420 nm is the bangap of ZnSe [59], the peak at 488 nm is the babgap of ZnS [60], and the peak at 595 nm is the $^4T_1$ - $^6A_1$ shift of the luminous center of Mn^{2+}.

The luminescence intensity at the Mn^{2+} core at 595 nm influences the luminescent properties of NCs. The fluorescence efficiency of ZnSe/ZnS:Mn/ZnS NCs exceeds that of ZnSe and ZnS. This can be explained by the following factors: The fluorescence efficiency of these NCs is low due to configurational aberrations in ZnSe and ZnS (Zn belongs to group IIB, S and Se belong to group VIA), as well as structural flaws. When doping Mn metal, adding a ZnS shell or buffer layer boosts the fluorescence intensity of NCs. Because ZnS acts as a buffer layer in ZnSe/ZnS:Mn/ZnS NCs, the effect of the ZnS buffer layer is to reduce the difference in lattice constant between the core and the shell, thereby reducing stress at the interface between the core and the shell, resulting in the reduction of surface defects of NCs caused by stress, and will significantly increase the fluorescence efficiency [61]. Furthermore, NCs will not be ionized, the ZnS shell barrier surrounding the NCs core will limit the trapped carriers on the surface, and adding a shell of a semiconductor with a larger band gap (such as ZnS with a band gap of ZnSe) can increase quantum efficiency and improve

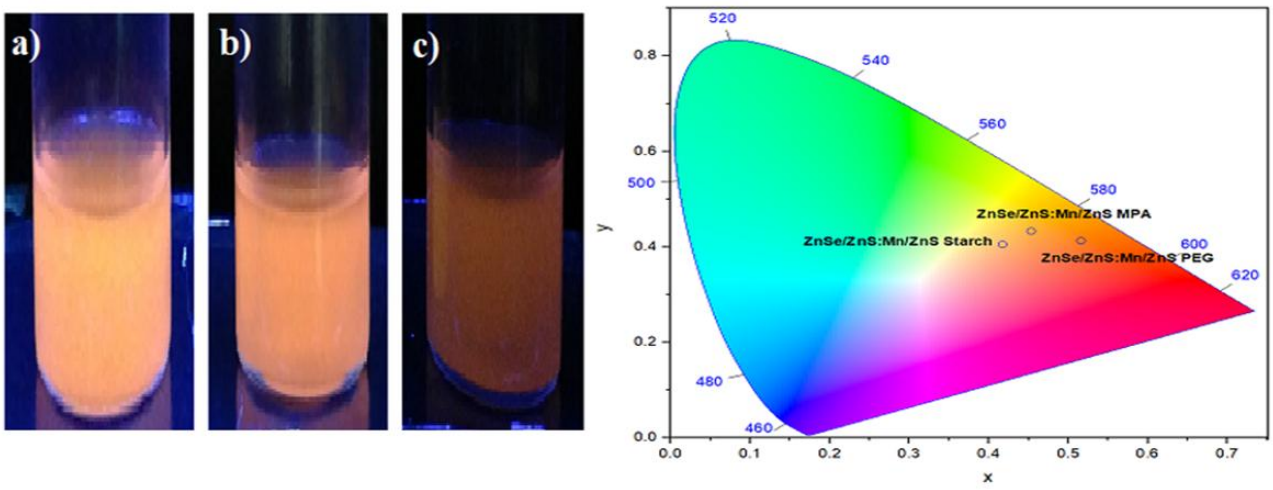

Figure 8. Image of ZnSe/ZnS:Mn/ZnS MPA NCs a), ZnSe/ZnS:Mn/ZnS PEG NCs b), ZnSe/ZnS:Mn/ZnS Starch NCs c) and CIE color coordinate of NCs synthesized using different surface stabilizers.

their stability [61,62]. The ZnSe/ZnS:Mn/ZnS MPA NCs with core/shell/spacer structures outperformed ZnSe/ZnS:Mn/ZnS Starch NCs and ZnSe/ZnS:Mn/ZnS PEG NCs in terms of fluorescence performance. Because of its short linear chain structure, MPA is well-suited to forming bonds with NCs surface atoms and complexes with doped metal ions [63,64]. One MPA molecule can connect with a metal atom site to form the best hexagonal configuration and increase the colloidal stability of the generated NCs, which improves fluorescence performance over PEG and starch.

In nano ZnSe/ZnS:Mn/ZnS PEG, PEG is a polyether chain that can absorb water and establish hydrogen bonds, allowing for solubility in polar solvents and stabilizing the colloid in acidic or basic pH conditions [30]. PEG molecules are long, straight chains (zigzags). However, when PEG dissolves in water, it forms pentacyclic rings (denutural geometry). A significant quantity of activated oxygen resides in the PEG molecular chain, resulting in strong contacts between PEG molecules and metal ions, particularly transition metal ions, PEG functions as a shell [65,66]. As a result, when we add a ZnS shell to the NCs, we mistakenly add a second shell (the first shell is the PEG itself) (Scheme 1). This thick shell reduces the fluorescence intensity of the NCs by blocking the excitation energy of the Mn^{2+} luminescent core.

Amylose is a linear polysaccharide made of glucose units connected by α-1,4-glycosidic linkages. Amylose molecules contain one reducing and one non-reducing end. Amylose molecular chains twist in a coiled pattern. The coiled shape is caused by the creation of hydrogen bonds between glucose units. Each helix contains six glucose units and is held together by hydrogen connections to adjacent helices. The space between the helices is large enough to bind to a variety of different molecules. Amylose only takes on its helical form in solution at ambient temperature. At high temperatures, the helix straightens and becomes unable to attach to other molecules [26,67].

Amylopectin is a branching polysaccharide. The main chain has α-1,4-glycosidic links, while branch chains are linked by α-1,6-glycosidic linkages. Amylopectin's complicated structure includes α-1,6-glycosidic bonds every 20-30 glucose units, resulting in a branch chain. From the first level branch chain, a second level branch chain is generated, and so forth. Amylopectin molecules branch at multiple levels [68] and contain nanocrystals, which reduces the excitation energy of the Mn^{2+} luminous center compared to MPA. The fluorescence quantum efficiency (Table 1) of NCs synthesized using surface stabilizers MPA, PEG, and Starch when using Rhodamine B as a standard with a fluorescence efficiency of 65% changed in the order: ZnSe/ZnS:Mn/ZnS MPA (73.95%) > ZnSe/ZnS:Mn/ZnS Starch (57.35%) > ZnSe/ZnS:Mn/ZnS-PEG (41.72%) > ZnSe (18.96%).

3.4. Research Into the Use of Materials for Bacterial Detection

3.4.1. Experimental results of the effect of NCs on bacterial growth

After manufacturing luminous nanoparticles and investigating the impact of surface stabilizers

Table 1. Fluorescence quantum efficiency of nanoparticles produced with various surface stabilizers ZnSe/ZnS:Mn/ZnS MPA; ZnSe/ZnS:Mn/ZnS PEG; ZnSe/ZnS:Mn/ZnS Starch and ZnSe.

Sample	Fluorescence quantum efficiency (%)
ZnSe/ZnS:Mn/ZnS MPA	73.95
ZnSe/ZnS:Mn/ZnS PEG	41.72
ZnSe/ZnS:Mn/ZnS Starch	57.35
ZnSe	18.96

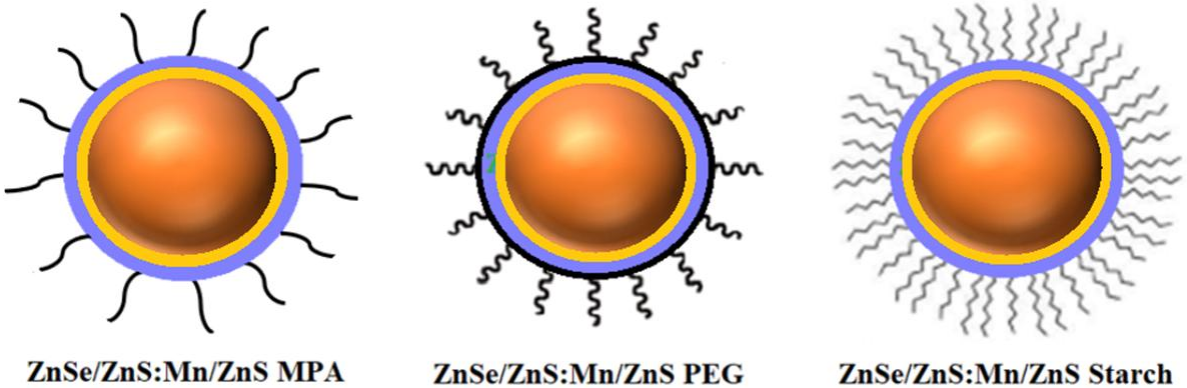

Scheme 1. Schematic representation of ZnSe/ZnS:Mn/ZnS nanoparticles synthesized using different surface stabilizers.

on material characteristics. We chose a representative sample with the highest fluorescence efficiency, ZnSe/ZnS:Mn/ZnS MPA, synthesized in an aqueous environment using MPA surface stabilizer, with a cubic crystal structure (zinc blende), spherical shape, and well dispersed in water, to test the applicability of NCs to quickly detect *E. coli O157:H7* bacteria.

Bacteria were dispersed on an agar plate with agar pores of 6 mm in diameter. Incubate the well with 20 mL of NCs solution for 24 hours at 37 °C. Figure 9a depicts the diffusion phenomenon on the agar medium. We can see that at the initial concentration of 10^{o} (sample 5) and the diluted NCs solution of 10^{-2} (sample 7), 10^{-3} (sample 8) has very little effect on the growth of *E.coli O157:H7* bacteria (Figure 9b), whereas the concentration of 10^{-1} has almost no effect on the growth of *E.coli O157:H7* bacteria. As a result, the sample with a concentration of 10^{-1} (sample 6) was chosen to determine the reaction's sensitivity and specificity.

3.4.2. Evaluation of NCs' ability in bacterial detection on E.*coli O157:H7* trains.

After assessing the toxicity of NCs against the *E. coli O157:H7* strain. These data suggested that NCs had little influence on the results of the subsequent investigation. Thus, NCs can be used to distinguish *E. coli O157:H7* strains. The compatibility of NCs with *E. coli O157:H7* bacteria was further assessed using fluorescence microscopy, with the findings shown in Figure 10. The complexes' morphology was recorded using fluorescence microscopy.

Fluorescence microscopy was used to capture the TEM imaging data and complicated structure (Figure 11). This image demonstrates that when NCs are linked to bacteria, they make the bacteria glow. Nanocrystals that do not adhere to bacteria will seem brighter than NCs that do. The findings indicate that NCs cling well to bacteria. As a result, they can be used to detect *E. coli O157:H7* bacterium.

4. Conclusions

We effectively generated ZnSe/ZnS:Mn/ZnS nanocrystals in an aqueous media with surface stabilizers MPA (short linear chain), PEG (long chain), and Stacrh (linear and branched chain). ZnSe/ZnS:Mn/ZnS NCs are spherical in shape, well dispersed in water, and nontoxic. When exposed to 365 nm UV light, ZnSe/ZnS:Mn/ZnS NCs appear orange-yellow. Changing the surface stabilizer and metal doping does not alter the structure of the ZnSe substrate material, but does improve its fluorescence performance. ZnSe/ZnS:Mn/ZnS MPA NCs exhibits better fluorescence performance than ZnSe/ZnS:Mn/ZnS PEG NCs and ZnSe/ZnS:Mn/ZnS Starch NCs. The ZnSe/ZnS:Mn/ZnS MPA NCs were evaluated and shown to be non-toxic to *E. coli O157:H7* bacteria, making them useful for detecting the intestinal pathogen. The study's findings may be valuable in the manufacturing of nanomaterials using green synthesis, which uses low-cost, non-toxic, and environmentally friendly raw materials, as well as in expanding the variety of nanomaterial applications in biomedicine.

Acknowledgment

The authors acknowledge the Industrial University of Ho Chi Minh City, Vietnam for supporting this work (funding no. 23.1HH03).

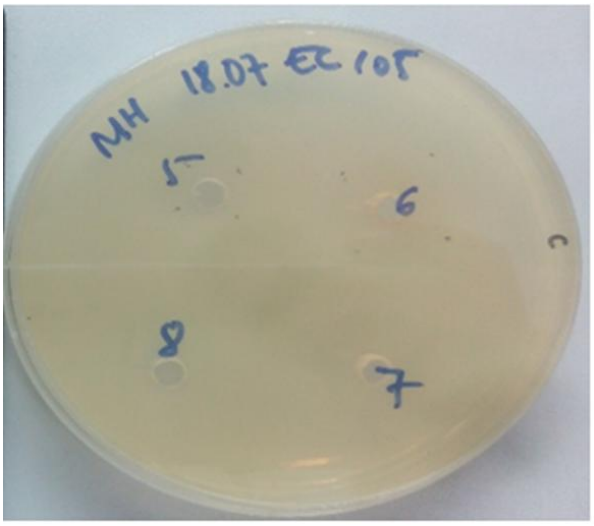

Figure 10. Results of interaction between NCs and *E. coli O157:H7* bacteria at a concentration of 10^5 CFU/mL at various concentrations of (10^{o}, 10^{-1}, 10^{-2}, 10^{-3}), named 5, 6, 7, 8 samples.

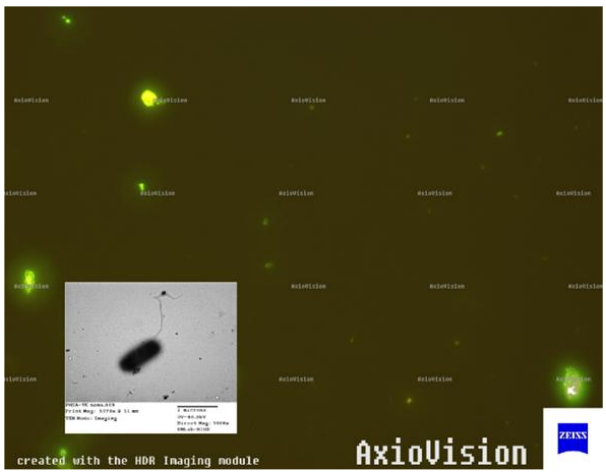

Figure 11. A fluorescence microscope photograph of *E. coli O157:H7* strains.

CRedit Author Statement

Author Contributions: Thi Diem Bui (Conceptualization, Writing - Review & Editing, Supervision), Quang Liem Nguyen (Writing - Original Draft), Nguyen Van Cuong (Data Curation, Writing - Original Draft), Trong Tang Nguyen (Data Curation).. All authors have read and agreed to the published version of the manuscript.

References

[1] Van, H.T., Vinh, N.D., Ca, N.X., Hien, N.T., Luyen, N.T., Do, P.V., Khien, N.V. (2020). Effects of ligand and chemical affinity of S and Se precursors on the shape, structure and optical properties of ternary CdS1−xSex alloy nanocrystals. *Materials Letters*, 264, 127387. DOI: 10.1016/j.matlet.2020.127387.

[2] Ca, N.X., Van, H.T., Do, P. V., Thanh, L.D., Tan, P.M., Truong, N.X., Oanh, V.T.K., Binh, N.T., Hien, N.T. (2020). Influence of precursor ratio and dopant concentration on the structure and optical properties of Cu-doped ZnCdSe-alloyed quantum dots. *RSC Advances*, 10(43), 25618–25628. DOI: 10.1039/D0RA04257A.

[3] Das, S., Mandal, K.C. (2012). Optical downconversion in rare earth (Tb3+ and Yb3+) doped CdS nanocrystals. *Materials Letters*, 66(1), 46–49. DOI: 10.1016/j.matlet.2011.08.034.

[4] Senthilkumar, K., Kalaivani, T., Kanagesan, S., Balasubramanian, V. (2012). Synthesis and characterization studies of ZnSe quantum dots. *Journal of Materials Science: Materials in Electronics*, 23(11), 2048–2052. DOI: 10.1007/s10854-012-0701-1.

[5] Zhao, Y., Yang, C., Zhang, S., Sun, G., Zhu, B., Wang, L., Zhang, J. (2024). Investigating the charge transfer mechanism of ZnSe QD/COF S-scheme photocatalyst for H2O2 production by using femtosecond transient absorption spectroscopy. *Chinese Journal of Catalysis*, 63, 258–269. DOI: 10.1016/S1872-2067(24)60069-0.

[6] Vempuluru, N.R., Kwon, H., Parnapalle, R., Urupalli, B., Munnelli, N., Lee, Y., Marappan, S., Mohan, S., Murikinati, M.K., Muthukonda Venkatakrishnan, S., Kim, K., Ahn, C.W., Yang, J.-M. (2024). ZnS/ZnSe heterojunction photocatalyst for augmented hydrogen production: Experimental and theoretical insights. *International Journal of Hydrogen Energy*, 51, 524–539. DOI: 10.1016/j.ijhydene.2023.08.249.

[7] Baum, F., da Silva, M.F., Linden, G., Feijo, D., Rieder, E.S., Santos, M.J.L. (2019). Growth dynamics of zinc selenide quantum dots: the role of oleic acid concentration and synthesis temperature on driving optical properties. *Journal of Nanoparticle Research*, 21(2), 42. DOI: 10.1007/s11051-019-4485-6.

[8] Lin, S., Li, J., Pu, C., Lei, H., Zhu, M., Qin, H., Peng, X. (2020). Surface and intrinsic contributions to extinction properties of ZnSe quantum dots. *Nano Research*, 13(3), 824–831. DOI: 10.1007/s12274-020-2703-2.

[9] Zahra, T., Alanazi, M.M., Alahmari, S.D., Abdelmohsen, S.A.M., Abdullah, M., Aman, S., Al-Sehemi, A.G., Henaish, A.M.A., Ahmad, Z., Tahir Farid, H.M. (2024). Hydrothermally synthesized ZnSe@FeSe nanocomposite: A promising candidate for energy storage devices. *International Journal of Hydrogen Energy*, 59, 97–106. DOI: 10.1016/j.ijhydene.2024.01.293.

[10] El-assar, M., Taha, T.E., El-Samie, F.E.A., Fayed, H.A., Aly, M.H. (2023). ZnSe-based highly-sensitive SPR biosensor for detection of different cancer cells and urine glucose levels. *Optical and Quantum Electronics*. 55 (1), 76. DOI: 10.1007/s11082-022-04326-y.

[11] Pechstedt, K., Whittle, T., Baumberg, J., Melvin, T. (2010). Photoluminescence of Colloidal CdSe/ZnS Quantum Dots: The Critical Effect of Water Molecules. *The Journal of Physical Chemistry C*, 114(28), 12069–12077. DOI: 10.1021/jp100415k.

[12] Yu, J.H., Kim, J., Hyeon, T., Yang, J. (2019). Facile synthesis of manganese (II)-doped ZnSe nanocrystals with controlled dimensionality. *The Journal of Chemical Physics*, 151(24) DOI: 10.1063/1.5128511.

[13] Yao, J.H., Elder, K.R., Guo, H., Grant, M. (1993). Theory and simulation of Ostwald ripening. *Physical Review B*, 47(21), 14110–14125. DOI: 10.1103/PhysRevB.47.14110.

[14] Winiarz, J.G., Zhang, L., Lal, M., Friend, C.S., Prasad, P.N. (1999). Photogeneration, charge transport, and photoconductivity of a novel PVK/CdS-nanocrystal polymer composite. *Chemical Physics*, 245(1–3), 417–428. DOI: 10.1016/S0301-0104(99)00057-9.

[15] Qi, L., Cölfen, H., Antonietti, M. (2001). Synthesis and Characterization of CdS Nanoparticles Stabilized by Double-Hydrophilic Block Copolymers. *Nano Letters*, 1(2), 61–65. DOI: 10.1021/nl0055052.

[16] Lee, Y.-J., Kim, T.-G., Sung, Y.-M. (2006). Lattice distortion and luminescence of CdSe/ZnSe nanocrystals. *Nanotechnology*, 17(14), 3539–3542. DOI: 10.1088/0957-4484/17/14/030.

[17] Jadhav, S.A. (2012). Functional self-assembled monolayers (SAMs) of organic compounds on gold nanoparticles. *Journal of Materials Chemistry*, 22(13), 5894. DOI: 10.1039/c2jm14239b.

[18] Ghosh Chaudhuri, R., Paria, S. (2012). Core/Shell Nanoparticles: Classes, Properties, Synthesis Mechanisms, Characterization, and Applications. *Chemical Reviews*, 112(4), 2373–2433. DOI: 10.1021/cr100449n.

[19] Huang, F., Peng, Y., Lin, C. (2006). Synthesis and Characterization of ZnS: Ag Nanocrystals Surface-capped with Thiourea1. *Chemical Research in Chinese Universities*, 22(6), 675–678. DOI: 10.1016/S1005-9040(06)60188-8.

[20] Raievska, O., Stroyuk, O., Dzhagan, V., Solonenko, D., Zahn, D.R.T. (2020). Ultra-small aqueous glutathione-capped Ag–In–Se quantum dots: luminescence and vibrational properties. *RSC Advances*, 10(69), 42178–42193. DOI: 10.1039/D0RA07706B.

[21] Basavaraj, U., Kumar, B.J., Mahesh, H.M. (2025). A Facile Synthesis of TGA Stabilized ZnSe Quantum Dots for Energy Harvesting Applications. In: Joseph D., P., V., J., Thangaraju, K. (eds) *Proceedings of the International Conference on Emerging Multifunctional Materials and Devices for Sustainable Technologies. IEMDST 2024*. Springer Proceedings in Physics, vol 567. Springer, Singapore. pp. 7–15. DOI: 10.1007/978-981-96-5863-3_2.

[22] Operamolla, A., Punzi, A., Farinola, G.M. (2017). Synthetic Routes to Thiol-Functionalized Organic Semiconductors for Molecular and Organic Electronics. *Asian Journal of Organic Chemistry*, 6(2), 120–138. DOI: 10.1002/ajoc.201600460.

[23] Choi, M.G., Cho, M.J., Ryu, H., Hong, J., Chang, S.-K. (2017). Fluorescence signaling of thiophenol by hydrolysis of dinitrobenzenesulfonamide of 2-(2-aminophenyl)benzothiazole. *Dyes and Pigments*, 143, 123–128. DOI: 10.1016/j.dyepig.2017.04.026.

[24] Castro, J. V., Dumas, C., Chiou, H., Fitzgerald, M.A., Gilbert, R.G. (2005). Mechanistic Information from Analysis of Molecular Weight Distributions of Starch. *Biomacromolecules*, 6(4), 2248–2259. DOI: 10.1021/bm0500401.

[25] Singh, J., Kaur, L., McCarthy, O.J. (2007). Factors influencing the physico-chemical, morphological, thermal and rheological properties of some chemically modified starches for food applications—A review. *Food Hydrocolloids*, 21(1), 1–22. DOI: 10.1016/j.foodhyd.2006.02.006.

[26] Radosta, S., Haberer, M., Vorwerg, W. (2001). Molecular Characteristics of Amylose and Starch in Dimethyl Sulfoxide. *Biomacromolecules*, 2(3), 970–978. DOI: 10.1021/bm0100662.

[27] Villwock, K., BeMiller, J.N. (2022). The Architecture, Nature, and Mystery of Starch Granules. Part 2. *Starch - Stärke*, 74(11–12) DOI: 10.1002/star.202100184.

[28] Lane, M.E. (2011). Nanoparticles and the skin – applications and limitations. *Journal of Microencapsulation*, 28(8), 709–716. DOI: 10.3109/02652048.2011.599440.

[29] Cole, A.J., David, A.E., Wang, J., Galbán, C.J., Yang, V.C. (2011). Magnetic brain tumor targeting and biodistribution of long-circulating PEG-modified, cross-linked starch-coated iron oxide nanoparticles. *Biomaterials*, 32(26), 6291–6301. DOI: 10.1016/j.biomaterials.2011.05.024.

[30] Gamucci, O., Bertero, A., Gagliardi, M., Bardi, G. (2014). Biomedical Nanoparticles: Overview of Their Surface Immune-Compatibility. *Coatings*, 4(1), 139–159. DOI: 10.3390/coatings4010139.

[31] Final Report on the Safety Assessment of Polyethylene Glycols (PEGs)-6,-8,-32,-75,-150,-14M,-20M. (1993). *Journal of the American College of Toxicology*. 12(5), 429-457. DOI: 10.3109/10915819309141598.

[32] Dreborg, S., Akerblom, E.B. (1990). Immunotherapy with monomethoxypolyethylene glycol modified allergens. *Critical Reviews in Therapeutic Drug Carrier Systems*, 6(4), 315–365.

[33] Yamaoka, T., Tabata, Y., Ikada, Y. (1994). Distribution and Tissue Uptake of Poly(ethylene glycol) with Different Molecular Weights after Intravenous Administration to Mice. *Journal of Pharmaceutical Sciences*, 83(4), 601–606. DOI: 10.1002/jps.2600830432.

[34] Blume, G., Cevc, G. (1993). Molecular mechanism of the lipid vesicle longevity in vivo. *Biochimica et Biophysica Acta (BBA) - Biomembranes*, 1146 (2), 157–168. DOI: 10.1016/0005-2736(93)90351-Y.

[35] Torchilin, V.P., Omelyanenko, V.G., Papisov, M.I., Bogdanov, A.A., Trubetskoy, V.S., Herron, J.N., Gentry, C.A. (1994). Poly(ethylene glycol) on the liposome surface: on the mechanism of polymer-coated liposome longevity. *Biochimica et Biophysica Acta (BBA) - Biomembranes*, 1195(1), 11–20. DOI: 10.1016/0005-2736(94)90003-5.

[36] Thi Luong, B., Hyeong, E., Ji, S., Kim, N. (2012). Green synthesis of highly UV-orange emitting ZnSe/ZnS:Mn/ZnS core/shell/shell nanocrystals by a three-step single flask method. *RSC Advances*, 2(32), 12132. DOI: 10.1039/c2ra21309e.

[37] Lan, G.-Y., Lin, Y.-W., Huang, Y.-F., Chang, H.-T. (2007). Photo-assisted synthesis of highly fluorescent ZnSe(S) quantum dots in aqueous solution. *Journal of Materials Chemistry*, 17(25), 2661. DOI: 10.1039/b702469j.

[38] Lesnyak, V., Plotnikov, A., Gaponik, N., Eychmüller, A. (2008). Toward efficient blue-emitting thiol-capped Zn1−xCdxSe nanocrystals. *Journal of Materials Chemistry*, 18(42), 5142. DOI: 10.1039/b811859k.

[39] Pathak, S., Davidson, M.C., Silva, G.A. (2007). Characterization of the Functional Binding Properties of Antibody Conjugated Quantum Dots. *Nano Letters*, 7(7), 1839–1845. DOI: 10.1021/nl062706i.

[40] Song, F., Chan, W.C.W. (2011). Principles of conjugating quantum dots to proteins via carbodiimide chemistry. *Nanotechnology*, 22(49), 494006. DOI: 10.1088/0957-4484/22/49/494006.

[41] Qiao, F., Kang, R., Liang, Q., Cai, Y., Bian, J., Hou, X. (2019). Tunability in the Optical and Electronic Properties of ZnSe Microspheres via Ag and Mn Doping. *ACS Omega*, 4(7), 12271–12277. DOI: 10.1021/acsomega.9b01539.

[42] Yousefi, R., Azimi, H.R., Mahmoudian, M.R., Basirun, W.J. (2018). The effect of defect emissions on enhancement photocatalytic performance of ZnSe QDs and ZnSe/rGO nanocomposites. *Applied Surface Science*, 435, 886–893. DOI: 10.1016/j.apsusc.2017.11.183.

[43] Tavakkoli Yaraki, M., Tayebi, M., Ahmadieh, M., Tahriri, M., Vashaee, D., Tayebi, L. (2017). Synthesis and optical properties of cysteamine-capped ZnS quantum dots for aflatoxin quantification. *Journal of Alloys and Compounds,* 690, 749–758. DOI: 10.1016/j.jallcom.2016.08.158.

[44] Geszke, M., Murias, M., Balan, L., Medjahdi, G., Korczynski, J., Moritz, M., Lulek, J., Schneider, R. (2011). Folic acid-conjugated core/shell ZnS:Mn/ZnS quantum dots as targeted probes for two photon fluorescence imaging of cancer cells. *Acta Biomaterialia*, 7(3), 1327–1338. DOI: 10.1016/j.actbio.2010.10.012.

[45] Geszke, M., Murias, M., Balan, L., Medjahdi, G., Korczynski, J., Moritz, M., Lulek, J., Schneider, R. (2011). Folic acid-conjugated core/shell ZnS:Mn/ZnS quantum dots as targeted probes for two photon fluorescence imaging of cancer cells. *Acta Biomaterialia*, 7(3), 1327–1338. DOI: 10.1016/j.actbio.2010.10.012

[46] Qu, L., Peng, X. (2002). Control of Photoluminescence Properties of CdSe Nanocrystals in Growth. *Journal of the American Chemical Society*, 124(9), 2049–2055. DOI: 10.1021/ja017002j.

[47] Califano, M., Franceschetti, A., Zunger, A. (2005). Temperature Dependence of Excitonic Radiative Decay in CdSe Quantum Dots: The Role of Surface Hole Traps. *Nano Letters*, 5(12), 2360–2364. DOI: 10.1021/nl051027p.

[48] Reiss, P., Protière, M., Li, L. (2009). Core/Shell Semiconductor Nanocrystals. *Small*, 5(2), 154–168. DOI: 10.1002/smll.200800841.

[49] Califano, M., Franceschetti, A., Zunger, A. (2005). Temperature Dependence of Excitonic Radiative Decay in CdSe Quantum Dots: The Role of Surface Hole Traps. *Nano Letters*, 5(12), 2360–2364. DOI: 10.1021/nl051027p.

[50] Reiss, P., Protière, M., Li, L. (2009). Core/Shell Semiconductor Nanocrystals. *Small*, 5(2), 154–168. DOI: 10.1002/smll.200800841.

[51] Talapin, D. V., Mekis, I., Götzinger, S., Kornowski, A., Benson, O., Weller, H. (2004). CdSe/CdS/ZnS and CdSe/ZnSe/ZnS Core−Shell−Shell Nanocrystals. *The Journal of Physical Chemistry B*, 108(49), 18826–18831. DOI: 10.1021/jp046481g.

[52] Talapin, D. V., Rogach, A.L., Kornowski, A., Haase, M., Weller, H. (2001). Highly Luminescent Monodisperse CdSe and CdSe/ZnS Nanocrystals Synthesized in a Hexadecylamine−Trioctylphosphine Oxide−Trioctylphospine Mixture. *Nano Letters*, 1(4), 207–211. DOI: 10.1021/nl0155126.

[53] Li, C.L., Nishikawa, K., Ando, M., Enomoto, H., Murase, N. (2007). Highly luminescent water-soluble ZnSe nanocrystals and their incorporation in a glass matrix. *Colloids and Surfaces A: Physicochemical and Engineering Aspects*, 294(1–3), 33–39. DOI: 10.1016/j.colsurfa.2006.07.052.

[54] López-Esparza, J., Espinosa-Cristóbal, L.F., Donohue-Cornejo, A., Reyes-López, S.Y. (2016). Antimicrobial Activity of Silver Nanoparticles in Polycaprolactone Nanofibers against Gram-Positive and Gram-Negative Bacteria. *Industrial & Engineering Chemistry Research*, 55(49), 12532–12538. DOI: 10.1021/acs.iecr.6b02300.

[55] Cao, M., Wang, Y., Guo, C., Qi, Y., Hu, C., Wang, E. (2004). A Simple Route Towards CuO Nanowires and Nanorods. *Journal of Nanoscience and Nanotechnology*, 4(7), 824–828. DOI: 10.1166/jnn.2004.822.

[56] He, Y., Lu, H., Sai, L., Su, Y., Hu, M., Fan, C., Huang, W., Wang, L. (2008). Microwave Synthesis of Water-Dispersed CdTe/CdS/ZnS Core-Shell-Shell Quantum Dots with Excellent Photostability and Biocompatibility. *Advanced Materials*, 20(18), 3416–3421. DOI: 10.1002/adma.200701166.

[57] You, S., Fiedorowicz, M., Lim, S. (1999). Molecular Characterization of Wheat Amylopectins by Multiangle Laser Light Scattering Analysis. *Cereal Chemistry*, 76(1), 116–121. DOI: 10.1094/CCHEM.1999.76.1.116.

[58] Peng, Q.-J., Perlin, A.S. (1987). Observations on N.M.R. spectra of starches in dimethyl sulfoxide, iodine-complexing, and solvation in water-dimethyl sulfoxide. *Carbohydrate Research*, 160, 57–72. DOI: 10.1016/0008-6215(87)80303-8.

[59] Lee, G.-J., Anandan, S., Masten, S.J., Wu, J.J. (2014). Sonochemical Synthesis of Hollow Copper Doped Zinc Sulfide Nanostructures: Optical and Catalytic Properties for Visible Light Assisted Photosplitting of Water. *Industrial & Engineering Chemistry Research*, 53(21), 8766–8772. DOI: 10.1021/ie500663n.

[60] Nguyen, T.P., Lam, Q.V., Vu, T.B. (2018). Effects of precursor molar ratio and annealing temperature on structure and photoluminescence characteristics of Mn-doped ZnS quantum dots. *Journal of Luminescence*, 196, 359–367. DOI: 10.1016/j.jlumin.2017.12.060.

[61] Bansal, N., Mohanta, G.C., Singh, K. (2017). Effect of Mn2+ and Cu2+ co-doping on structural and luminescent properties of ZnS nanoparticles. *Ceramics International*, 43(9), 7193–7201. DOI: 10.1016/j.ceramint.2017.03.007.

[62] Kuzmin, A., Dile, M., Laganovska, K., Zolotarjovs, A. (2022). Microwave-assisted synthesis and characterization of undoped and manganese doped zinc sulfide nanoparticles. *Materials Chemistry and Physics*, 290, 126583. DOI: 10.1016/j.matchemphys.2022.126583.

[63] Murugadoss, G. (2011). Synthesis, optical, structural and thermal characterization of Mn2+ doped ZnS nanoparticles using reverse micelle method. *Journal of Luminescence*, 131(10), 2216–2223. DOI: 10.1016/j.jlumin.2011.03.048.

[64] Qiao, F., Kang, R., Liang, Q., Cai, Y., Bian, J., Hou, X. (2019). Tunability in the Optical and Electronic Properties of ZnSe Microspheres via Ag and Mn Doping. *ACS Omega*, 4(7), 12271–12277. DOI: 10.1021/acsomega.9b01539.

[65] Wang, Y., Cheng, J., Yu, S., Alcocer, E.J., Shahid, M., Wang, Z., Pan, W. (2016). Synergistic effect of N-decorated and Mn2+ doped ZnO nanofibers with enhanced photocatalytic activity. *Scientific Reports*, 6(1), 32711. DOI: 10.1038/srep32711.

[66] Li, C., Zhang, H., Cheng, C. (2016). CdS/CdSe co-sensitized 3D SnO2/TiO2 sea urchin-like nanotube arrays as an efficient photoanode for photoelectrochemical hydrogen generation. *RSC Advances*, 6(44), 37407–37411. DOI: 10.1039/C6RA02176J.

[67] Singh, A., Geaney, H., Laffir, F., Ryan, K.M. (2012). Colloidal Synthesis of Wurtzite Cu2 ZnSnS4 Nanorods and Their Perpendicular Assembly. *Journal of the American Chemical Society*, 134(6), 2910–2913. DOI: 10.1021/ja2112146.

[68] Xu, H.Y., Liu, Y.C., Xu, C.S., Liu, Y.X., Shao, C.L., Mu, R. (2006). Room-temperature ferromagnetism in (Mn, N)-codoped ZnO thin films prepared by reactive magnetron cosputtering. *Applied Physics Letters*, 88(24) DOI: 10.1063/1.2213929.